Pergamon

Int. J. Heat Mass Transfer. Vol. 41, No. 11, pp. 1499–1511, 1998

Printed in Great Britain
0017–9310/98 \$19.00+0.00

PII: S0017–9310(97)00277–9

Thermocapillary convection in two-layer systems

Q. S. LIU† and B. ROUX‡

Institut de Recherches sur les Phénoménes Hors d'Equilibre Université de la Méditerranée, CNRS UMR-6594, IRPHE–IMT, Technopole de Chateau-Gombert, F-13451 Marseille Cedex 20, France

and

M. G. VELARDE

Instituto Pluridisciplinar, Universidad Complutense, Paseo Juan XXIII, 1, 28040 Madrid, Spain

(*Received* 3 *October* 1996 *and in final form* 17 *July* 1997)

Abstract—This paper concerns a numerical study of the flow characteristics of thermocapillary convection in a system composed of two immiscible liquid layers subject to a temperature gradient along their interface. We consider the two-layer system: B_2O_3 (encapsulant) and GaAs (melt), for its experimental relevance in crystal growth by the directional solidification method. Two cases have been studied: a system with only one liquid interface (melt/encapsulant) and a system where the outer surface of encapsulant is open to air (and so, subject to a second thermocapillary force). Both the liquid–liquid interface and the outer surface are assumed to be undeformable and flat, which is a valid assumption according to earlier theoretical and experimental results. A 2-D numerical simulation of convection is carried out in a rectangular cavity by solving the system of Navier–Stokes equations using a finite difference method with a staggered grid for the pressure. Having in perspective a Spacelab experimentation we disregarded gravity ($g = 0$). We show that a strong damping of the melt flow can be obtained by using an encapsulant liquid layer having appropriate viscosity, heat conductivity and/or thickness.

1. INTRODUCTION

The study of convective flows and heat transfers in a system of immiscible liquid layers has a great potential, due to numerous engineering applications, particularly for the liquid encapsulation technique of crystal growth by directional solidification. Encapsulation of an electronic melt is used to control melt stoichiometry when the melt contains a volatile component such as germanium, GaAs, etc. (see, for example, Metz *et al.* [1]). In addition, encapsulation can be useful for a better control of heat transfer as shown by Johnson [2]. It has also the advantage of reducing (or even eliminating) convective flow in the melt hence drastically reducing unwanted inhomogeneities in solidifying materials. The liquid encapsulated floating zone technique for space processing of high-purity semiconductors has been proposed by Barocela and Jalilevand [3]. In a microgravity environment, aboard a spacecraft, thermocapillary flows (induced by the Marangoni effect, i.e. by a surface stress due to the variation of surface tension with temperature along an interface) is of major importance as buoyancy is greatly reduced. To study the role of the liquid encapsulant on the possible damping of the melt flow, we consider a differentially heated system of two immiscible liquid layers open to air, hence a system with a liquid–liquid interface and a free top surface. We provide detailed numerical predictions of thermocapillary convection in such a two-layer system, with particular attention on the metallic melt GaAs, a low Prandtl number fluid covered by a layer of a highly viscous fluid (B_2O_3) which is the encapsulant liquid open to air. Although this configuration does not strictly correspond to the set-ups used by crystal growers, it captures, however, the essence of the problem and it allows us to obtain relevant information about the expected role of the encapsulant liquid.

Thermocapillary convection and heat transport phenomena in a two-layer system is complex due to the hydrodynamic and thermal interactions between fluids in the two contiguous layers and to Marangoni effect acting on both the liquid–liquid interface and the free top surface. In the crystal growth method with liquid-encapsulated floating-zones, the thermal gradient has two components: parallel and perpendicular to the liquid–liquid interface hence the possibility of 'thermocapillary convection' and 'convective instability', respectively. Here we study only the former case.

† Present address: National Microgravity Laboratory, Institute of Mechanics, CAS, Beijing 100080, China.

‡ Author to whom correspondence should be addressed.

NOMENCLATURE

A	aspect ratio (of the lower layer), L/H_2
g	acceleration of gravity
H_i	height of ith layer
H	total height of cavity (H_1+H_2)
L	length of cavity
Ma	Marangoni number, $\gamma_{2-1}\Delta TH_2^2/(\mu_2\kappa_2 L)$
p	dimensionless pressure
Pr	Prandtl number, ν_2/κ_2
T_c	constant temperature at cold wall
T_h	constant temperature at hot wall
ΔT	maximum temperature difference $(T_h - T_c)$
u, v	dimensionless velocity components
U_i	dimensionless horizontal velocity at interface
x, y	dimensionless Cartesian coordinates.

Greek symbols

γ	surface tension coefficient, $-\partial\sigma/\partial T$
θ	dimensionless temperature
κ	thermal diffusivity
λ	thermal conductivity
μ	dynamic viscosity
ν	kinematic viscosity
ρ	density
σ	surface tension
σ^*	surface-tension coefficient ratio of free surface to interface, $\gamma_{1-\mathrm{air}}/\gamma_{2-1}$
ψ	dimensionless streamfunction.

Superscripts

*	relative quantities (layer 1 to layer 2)
air	ambient condition (air).
i	ith fluid layer ($i = 1, 2$)

Earth-based experimental results exist about thermocapillary convection in a two layer system. For instance, Villers and Platten [4, 5], investigated thermocapillary and buoyancy-driven convection for a system of heptanol over water ($Pr \approx 7$) in a cavity, hence, no open surface to air. They measured the longitudinal (horizontal) velocity profiles in each layer and the interfacial tension profiles as a function of temperature along the interface. The convective flows have been also observed for different values of the two-layer thickness ratio. Also for a two-layer system in a cavity, Koster *et al.* [6] obtained experimental results including flow visualisation for the FC70-Sil0cS and FC70-Si50cS systems. Similar experiments were performed by Azuma *et al.* [7] but in a much shallower cavity open to air ($A = H/L > 20$) hence reducing the influence of buoyancy. They observed a multi-cellular flow structure in the upper layer, where evaporation occurred at the top surface.

There also exist theoretical studies dealing with an asymptotic (1-D) problem for a two layer system, which can only provide understanding of convection far from the boundaries of the cavity. For instance, Villers and Platten [4], Napolitano *et al.* [8] and Wang *et al.* [9] studied thermocapillary and buoyancy-driven convection. Shevtsova *et al.* [10] and Liu *et al.* [11] have studied the same geometry but with an open surface. All reports provided horizontal velocity and temperature profiles in a vertical cross-section of the cavity. Particular cases, with appropriate choice of parameters permitted studying conditions to reduce convection in the encapsulated layer or along the interface. Doi and Koster [12] restricted consideration to pure thermocapillary convection with a free top surface. Most of the theoretical analyses assume rectangular cavities of infinite aspect ratio ($A \to \infty$), for low Grashof and Marangoni numbers ($Gr \leqslant 1$ and $Ma \leqslant 1$).

A 2-D numerical investigation of combined thermocapillary and buoyancy-driven convection in two-layer systems of finite aspect ratio ($A < \infty$) heated from the side has been done by Liu *et al.* [11] and Liu [13], and Doi and Koster [12]. Their findings confirmed previous theoretical results for infinite aspect ratio layers that indeed the convection in the encapsulated layer (representing the melt) can be significantly reduced by a suitable choice of encapsulant liquid. Numerical studies in a rectangular cavity can be found also in refs. [14, 15]. In these papers the finite element code FIDAP was used. It was shown that a microgravity environment significantly reduces the flow in the system of water over fluorinet FC75 with a free top surface. It was also found that the deformation of both interfaces is negligible even for large Marangoni numbers, relative to fluid depth (smaller than 1/2000 for 1 g, and 1/180 for $10^{-5}\,g$, respectively).

A numerical study of combined thermocapillary and buoyancy-driven convection in a vertical two-layer cavity with a deformable liquid–liquid interface has been performed by Li *et al.* [16]. Their results show a strong reduction of the melt flow (GaAs) when the encapsulant is highly viscous (B_2O_3; the maximum flow velocity at the interface being reduced by a factor of 1000). Finally, let us mention the 2-D numerical study of Doi and Koster [12], to estimate the endwall effect in the case of a system of melt ($Pr = 0.01$) and encapsulant ($Pr = 1$) of equal depths.

The present paper is a continuation of an earlier work presented in the same journal (see Liu *et al.* [11]), but now attention is focused on a two-layer system corresponding to a metallic melt (GaAs) encapsulated by a highly viscous fluid (B_2O_3). This

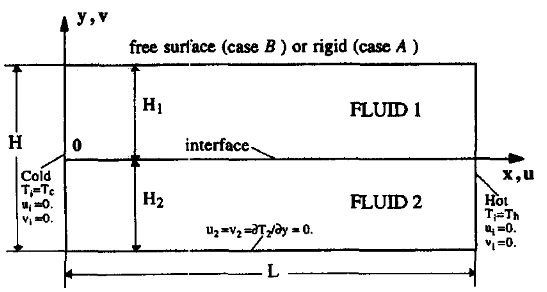

Fig. 1. Geometry and coordinate system of the problem.

system is contained in a rectangular cavity, laterally heated (see Fig. 1). We consider two cases for the outer surface of encapsulant, which is either confined by a rigid surface (quartz, for example) or not; in the later case, we account for a second thermocapillary effect able to counteract the one at the melt–encapsulant interface. For simplicity and due to the negligible value of the interface deformation, according to Sen and Davis [17] results, we consider both the liquid–liquid interface and open surface as undeformable. Before embarking in the study of the B_2O_3–GaAs system, we elucidate the specific influence on the thermocapillary flow played by the various parameters of the problem. In Section 3 we consider a rigid cavity (not open surface) with fluids of equal transport properties (Section 3.1), then with liquids of different transport properties, i.e. different viscosities (Section 3.2) and/or diffusivities (Section 3.3). Section 4 deals with the B_2O_3–GaAs system, which is a case of experimental relevance to crystal growth. In Section 4.1 we consider a rigid cavity, while in Section 4.2 the surface of the encapsulant (B_2O_3) is taken open to air, and, finally, in Section 4.3 we consider an encapsulant with unrealistically low viscosity in order to sort up in a finite geometry the effects of viscosity in the bulk due to the no-slip condition at the boundaries.

2. STATEMENT OF THE PROBLEM AND NUMERICAL METHOD

Let us consider a system of two immiscible and incompressible viscous fluids, liquid-1 (upper) and liquid-2 (lower), in a two-dimensional cavity of length L and height H as shown in Fig. 1. The thickness of the upper layer is H_1, and that of the lower layer is H_2; the total thickness is denoted H. The thickness ratio is $h^* = H_1/H_2$, and the lower-layer aspect ratio is $A = L/H_2$. The dynamic and kinematic viscosities, the density, the thermal conductivity and the thermal diffusivity of liquid-i are denoted μ_i, ν_i, ρ_i, λ_i and κ_i, respectively ($i = 1,2$). The rectangular cavity has a rigid bottom, a flat liquid–liquid interface and two types of boundary conditions for the top surface: (1) rigid plate (case A below); and (2) free surface subject to thermocapillary effect (case B). The vertical sidewalls of the cavity are maintained at constant temperatures T_c and T_h, where $T_c < T_h$; this yields an external temperature gradient parallel to the liquid–liquid interface. We assume that the horizontal walls are poorly conducting plates, and that the free top surface (for case B) is undeformable. For simplicity, no external force is considered (in particular, $g = 0$). The surface tension is assumed to vary linearly with temperature. At the interface between the two liquids we have:

$$\sigma_{2-1} = \sigma_{2-1_0} - \gamma_{2-1}(T_2 - T_0) \tag{1}$$

with $T_0 = (T_c + T_h)/2$ and $\gamma_{2-1} = -\partial\sigma_{2-1}/\partial T$, which is the temperature coefficient of interfacial tension. The subscript 0 denotes a reference state. In case B, it exists as a second surface-tension effect on the free top surface.

$$\sigma_{1-\mathrm{air}} = \sigma_{1-\mathrm{air}_0} - \gamma_{1-\mathrm{air}}(T_1 - T_0) \tag{2}$$

where $\gamma_{1-\mathrm{air}} = -\partial\sigma_{1-\mathrm{air}}/\partial T$ is the temperature coefficient of surface tension between liquid-1 and air.

The problem is rendered dimensionless by using H_2^2/κ_2, κ_2/H_2, H_2, $\Delta T H_2/L$ as new scales for, respectively, time, velocity, length and temperature, where $\Delta T = T_h - T_c$. The scaling factor for pressure is $\kappa_2^2\rho_2/H_2^2$.

The Navier–Stokes and energy equations have to be satisfied in each liquid layer of the system. Then, the flow is governed by the following dimensionless equations written in the form of primitive dependent variables as

$$\frac{\partial u_i}{\partial x} + \frac{\partial v_i}{\partial y} = 0 \tag{3}$$

$$\frac{\partial u_i}{\partial t} + u_i\frac{\partial u_i}{\partial x} + v_i\frac{\partial u_i}{\partial y} = -ZP_i\frac{\partial p_i}{\partial x} + ZD_i\left[\frac{\partial^2 u_i}{\partial x^2} + \frac{\partial^2 u_i}{\partial y^2}\right] \tag{4}$$

$$\frac{\partial v_i}{\partial t} + u_i\frac{\partial v_i}{\partial x} + v_i\frac{\partial v_i}{\partial y} = -ZP_i\frac{\partial p_i}{\partial y} - + ZD_i\left[\frac{\partial^2 v_i}{\partial x^2} + \frac{\partial^2 v_i}{\partial y^2}\right] \tag{5}$$

$$\frac{\partial \theta_i}{\partial t} + u_i\frac{\partial \theta_i}{\partial x} + v_i\frac{\partial \theta_i}{\partial y} = TD_i\left[\frac{\partial^2 \theta_i}{\partial x^2} + \frac{\partial^2 \theta_i}{\partial y^2}\right] \tag{6}$$

where $\theta_i = (T_i - T_c)L/\Delta T H_2$ ($i = 1,2$) is the dimensionless temperature. The 'constants' in the right hand side of these dimensionless equations (3)–(6) which depend on the choice of scaling quantities, are:

$$ZP_1 = \frac{1}{\rho^*};\quad ZD_1 = Pr\,\nu^*;\quad TD_1 = \kappa^*,$$

$$ZP_2 = 1;\quad ZD_2 = Pr;\quad TD_2 = 1.$$

The dimensionless coefficients in equations (3)–(6) contain the Prandtl number of the melt,

$$Pr = \nu_2/\kappa_2 \tag{7}$$

and the ratios of physical properties of liquid-1 to liquid-2:

$$\rho^* = \rho_1/\rho_2, \quad v^* = v_1/v_2 \quad \text{and} \quad \kappa^* = \kappa_1/\kappa_2.$$

At the solid walls (including the top wall, in case A), we take a no-slip boundary condition. At the cold and hot sidewalls, the temperature is differentially prescribed, and the bottom and the top rigid walls (for case A) are thermally poor conductors. At the flat interface, an the flat top surface in case B, the boundary conditions demand continuity of velocity and temperature, shear stress balance and heat flux balance. These boundary conditions are:

1. at the two vertical walls ($x = 0$ and $x = A$),

$$u_i = v_i = 0, \ \theta_i = 0 \ (\text{at}\, x = 0), \ \theta_i = A \ (\text{at}\, x = A) \quad (8)$$

2. at the rigid bottom ($y = -1$),

$$u_2 = v_2 = 0, \quad \frac{\partial \theta_2}{\partial y} = 0 \quad (9)$$

3. at the interface between layer-1 and layer-2 ($y = 0$),

$$u_1 = u_2, \quad v_1 = v_2 = 0, \quad \frac{\partial u_2}{\partial y} - \mu^* \frac{\partial u_1}{\partial y} = -Ma \frac{\partial \theta_2}{\partial x}$$

$$\theta_1 = \theta_2, \quad \lambda^* \frac{\partial \theta_1}{\partial y} = \frac{\partial \theta_2}{\partial y} \quad (10)$$

where

$$Ma = \gamma_{2-1} \Delta T H_2^2/(\mu_2 \kappa_2 L), \quad (11)$$

is the Marangoni number corresponding to the melt layer, λ^* is the ratio of thermal conductivites, $\lambda^* = \lambda_1/\lambda_2$.

4. at the top surface ($y = h^*$, with $h^* = H_1/H_2$), two cases are considered,

• for a rigid top surface (case A):

$$u_1 = v_1 = 0, \quad \frac{\partial \theta_1}{\partial y} = 0; \quad (12)$$

• for an open free top surface (case B):

$$v_1 = 0, \quad \mu^* \frac{\partial u_1}{\partial y} = -\sigma^* Ma \frac{\partial \theta_1}{\partial x},$$

$$\frac{\partial \theta_1}{\partial y} + Bi(\theta_1 - \theta_{\text{air}}) = 0, \quad (13)$$

where Bi is a Biot number and θ_{air} the ambient dimensionless temperature (for simplicity here we take $Bi = 0$);

$$\sigma^* = (-\partial \sigma_{1-\text{air}}/\partial T)/(-\partial \sigma_{2-1}/\partial T) \quad (14)$$

is the ratio of surface-tension temperature coefficients. The Marangoni number corresponding to the encapsulant layer is $Ma' = Ma(h^* \sigma^*/\mu^* \kappa^*)$.

The system of equations (3)–(6), with the appropriate boundary conditions equations (8)–(13), is solved by a finite difference method using an A.D.I. formulation to obtain a steady solution (see [13]). The convergence criterion for the Navier–Stokes equations is based on the maximum relative variation of variables (less than 0.01%). Most of the solutions reported below have been obtained on regular uniform meshes (from 31 to 201 nodes in the x-direction and from 21 to 35 nodes in the y-direction, for different aspect ratios, $1 \leqslant A \leqslant 12$). All computations were carried out in double precision on Intel-iPSC/860 computer. For the sake of completeness and to test the accuracy and convergence of our computer program we have performed calculations with non-vanishing gravity (see Table 1). For instance, for $A = 2$, $Gr = 10^4$, $h^* = \mu^* = Pr = 1$, $\lambda^* = 0.5$, $\kappa^* = 0.625$ and $\beta^* = 2$, our results using $51 \times (25+25)$ meshes agree quite satisfactorily with the results reported by Shevtsova et al. [18], who used a non-uniform regular mesh with 50×50 nodes for the spatial discretization.

3. THERMOCAPILLARY CONVECTION FOR MODEL OF TWO-LAYER SYSTEMS OF EQUAL DEPTH (CASE A)

The physical properties of liquid layers used in crystal growth experiments are often very different. These differences are expected to differently affect the velocity and temperature fields in each layer, even when the two layers have equal depth with symmetrical boundary conditions (both no-slip). Thus, let us see the role played by transport ratios. In this section the cavity has no open, free surface.

3.1. *'Symmetrical' system* ($\mu^* = \kappa^* = 1$)

From the analytical expressions of velocity profiles in an infinite aspect ratio cavity ($A \to \infty$) with $\mathbf{g} \neq 0$ (see Liu et al. [11]), we can derive an asymptotic solution of the dimensionless streamfunction of the system, for zero gravity ($\mathbf{g} = 0$). We have:

$$\psi_1 = -\frac{Ma\, C_T}{2(Q_\mu + 1)} \left(\frac{y^3}{h^{*2}} - 2\frac{y^2}{h^*} + y \right) + C_1 \qquad (0 \leqslant y \leqslant h^*) \quad (15)$$

$$\psi_2 = -\frac{Ma\, C_T}{4(Q_\mu + 1)} (y^3 - 2y^2 + y) + C_2 \qquad (-1 \leqslant y \leqslant 0) \quad (16)$$

where C_1 and C_2 are integration constants for the upper and lower layers, respectively, $Q_\mu = \mu^*/h^*$, and C_T represents the dimensionless value of the horizontal temperature gradient ($\partial \theta_i/\partial x$). We take $C_T = 1$, as the temperature field is assumed to linearly vary in x-direction for any y. As the streamfunction vanishes at rigid walls and at the interface, the values of the streamfunction can be obtained everywhere. In particular, we consider the absolute value of the streamfunction extremum in each layer, which represents

Table 1. Numerical results obtained for a two-layer system in both cases A and B at $A = 2$, $h^* = \mu^* = Pr = 1$, $\lambda^* = 0.5$, $\kappa^* = 0.625$, $\beta^* = 2$ (thermal expansion ratio) and $Gr = 10^4$ (Grashof number), $Re = 10^3$ (Reynolds number) (in case B), in comparison with those reported by Shevtsova *et al.* (1991)

Calculus case	Parameter	Present results (Shevtsova's)			
		$\Psi_{1,\max}$	$\Psi_{1,\min}$	$\Psi_{2,\max}$	$\Psi_{2,\min}$
Case A	$Re = 0$	1.804 (1.82)	0 (0)	1.280 (1.34)	−0.352 (?)
Case A	$Re = 10^3$	0.764 (0.78)	−1.041 (−1.08)	2.792 (2.87)	0 (0)
Case A	$Re = 10^4$	0.132 (?)	−12.92 (−12.79)	13.0 (12.90)	0 (0)
Case B	$\sigma^* = 0$	1.420 (1.40)	−0.970 (−0.99)	2.760 (2.84)	0 (0)
Case B	$\sigma^* = 1$	3.140 (3.16)	−0.820 (?)	2.720 (2.8)	0 (0)
Case B	$\sigma^* = 10$	18.36 (19.0)	−0.728 (?)	2.410 (2.5)	−0.156 (?)

the mass flow rate. For $Ma > 0$, it is equal to $|\psi_{1,\min}|$ in the encapsulant layer and to $\psi_{2,\max}$ in the melt layer, where:

$$\psi_{1,min} = -\frac{h^* Ma\, C_T}{27(Q_\mu+1)} \quad \text{at}\, y = \frac{h^*}{3} \tag{17}$$

$$\psi_{2,max} = \frac{Ma\, C_T}{27(Q_\mu+1)} \quad \text{at}\, y = -\frac{1}{3} \tag{18}$$

Expressions (7) and (8) show that if $h^* = 1$ (i.e., if the two layers have equal depth), the mass flow rate is the same in the two layers; i.e., $|\psi_{1,\min}| = |\psi_{2,\max}|$, for all Ma.

For finite cavities ($A = 4$) the computed values of the streamfunction for the fully-symmetric 2-D cases ($h^* = \kappa^* = \mu^* = \lambda^* = \rho^* = 1$ and $Pr_2 = 1$) are given in Fig. 2, in the range $10 \leqslant Ma \leqslant 1000$. As expected, the streamfunction in the upper layer is equal to that in the lower layer; in particular: $|\psi_{1,\min}| = |\psi_{2,\max}|$. The 2-D results coincide with the 1-D (asymptotic) expressions (17) and (18) only for very low Ma; for higher Ma the 2-D results tend to a parabolic evolution, in contrast with the linear 1-D solution. Of course, this difference between 1-D and 2-D solutions which is more evident for high Ma, comes from the increasing role played by the non-linearity in the finite cavity (which is absent in the 1-D solution).

The flow structure and isotherm patterns for the 2-D symmetrical model system are also shown in Fig. 2 for $Ma = 1000$. Like the 1-D analytical prediction, the numerical flow and temperature fields (streamlines and isotherms) in the two layers are perfectly symmetric with respect to the interface. In this case ($Ma = 1000$) the flow exhibits two juxtaposed, counter-rotating, vortices in each layer, thus leading to a strong modification of temperature field relative to the motionless, conducting case (vertical isotherms).

3.2. *Liquids of different viscosities* ($\mu_1 \neq \mu_2$; $\mu_2 =$ const.)

Three different encapsulant viscosities have been considered: $\mu^* = 0.1$, 10 and 100. The results can be compared to the case $\mu^* = 1$ in the range $50 \leqslant Ma \leqslant 10^4$. The computed streamlines and isotherms in the two layers are given for $\mu^* = 0.1$ and $\mu^* = 10$ in Fig. 3(a–b), respectively. The case $\mu^* > 1$ (i.e., where encapsulant viscosity is greater than melt viscosity) fits better for crystal growth experiments as it corresponds to a reduced velocity in the melt.

In Fig. 4 are given the variations of the maximum streamfunction (divided by Marangoni number) of the melt layer as a function of μ^* for different values of Ma ($Ma = 50$, 100, 500 and 1000). The solid line corresponds to analytical solution (18). It clearly appears that: (i) the convective flow intensity in both layers diminishes when increasing the viscosity of the upper layer, for all Ma; (ii) the effect of the lateral walls of the 2-D cavity are more evident for large values of Ma and for lower viscosity in the upper layer.

The thermocapillary flow structure when $\mu^* = 0.1$ is shown in Fig. 3(a) for $Ma = 1000$. At variance with the case $\mu^* = 1$ streamlines and isotherms in both layers are no longer symmetric with respect to the liquid–liquid interface. A typical 'flywheel' structure appears in the upper layer near the cold end-wall, and a longer and larger convective cell fills almost all the melt layer. Even with so different structures, the two major convective cells have about the same intensity (maximum streamfunction) both high. This situation has no experimental interest. The case $\mu^* \gg 1$ is the interesting one. For example, for $\mu^* = 100$ and $Ma = 10^4$, the extreme values of the calculated streamfunction are: $\psi_{1,\min} = -2.588$ for the encapsulant, and $\psi_{2,\max} = 2.876$ for the melt. In this case, the flow velocity is reduced and a parallel flow develops in most of the two layers (as in Fig. 3(b)).

3.3. *Liquids of different thermal diffusivities* (κ_1; $\kappa_2 = const.$)

Now, let us vary only the thermal diffusivity of liquid-1 (encapsulant) while that of liquid-2 (melt) is maintained constant. For illustration we take $\kappa_2 = 1$ and allow κ_1 to vary from 0.1 to 10. Flow patterns together with isotherms are shown for $\kappa^* = 0.1$ and $Ma = 500$, and for $\kappa^* = 10$ and $Ma = 1000$, in Fig. 5(a)–(b), respectively. Note that the flow fields in each

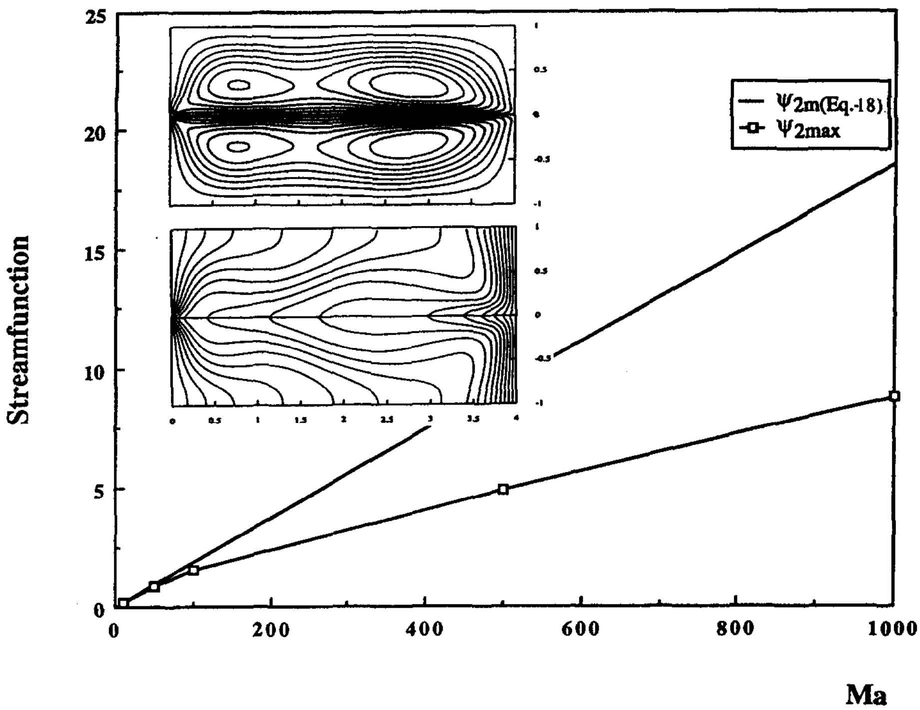

Fig. 2. Variation of $\psi_{2,max}/Ma$ as a function of Ma in case A, for a symmetric system $Pr_1 = Pr_2 = 1$, $h^* = \mu^* = \kappa^* = \rho^* = \lambda^* = 1$ and $A = 4$; and streamlines (above) and isotherms (below) for $Ma = 1000$.

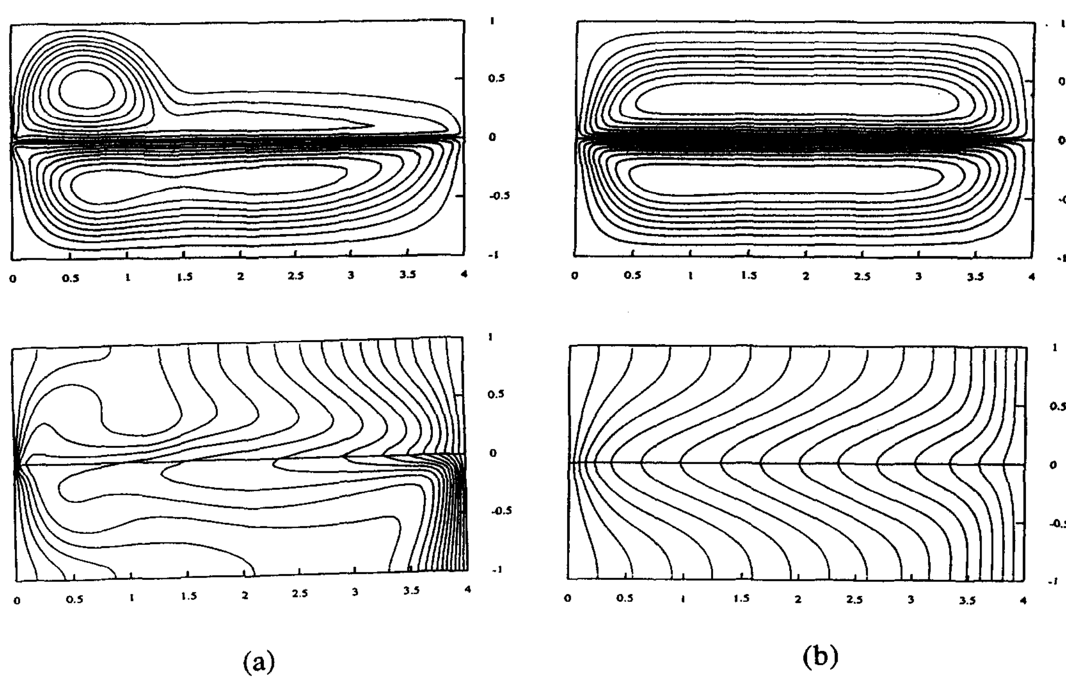

Fig. 3. Streamlines (above) and isotherms (below) for asymmetric systems ($\mu_1 \neq \mu_2$) at $Pr_2 = h^* = \kappa^* = \rho^* = \lambda^* = 1$ and $A = 4$; and streamlines (a) for $\mu^* = 0.1$, (b) $\mu^* = 10$, $Ma = 1000$.

layer appear to be fully symmetric with respect to the interface; in particular we have the same mass flow rate in each layer, i.e., $\psi_{2,max} = -\psi_{1,min}$. This is due to the fact that the Marangoni effect, the only driving force (along the interface) produces identical flow effect in the two layers. Indeed the viscous effect are

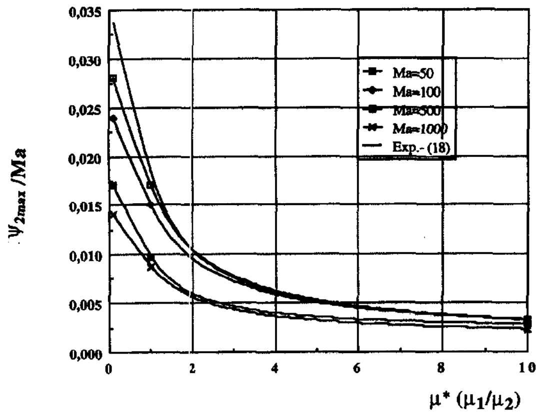

Fig. 4. Evolution of $\psi_{2,\max}/Ma$ as a function of μ^* for different values of Ma, at $Pr_2 = h^* = \mu^* = \rho^* = \lambda^* = 1$ and $A = 4$.

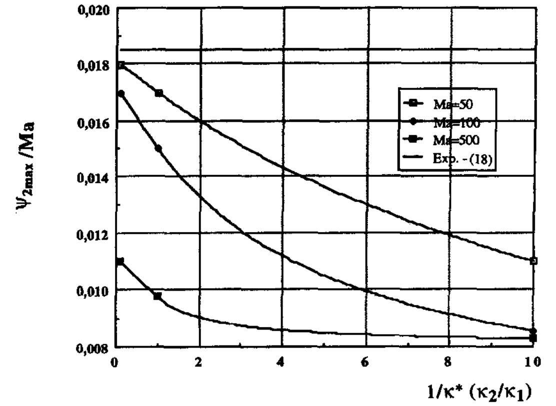

Fig. 6. Evolution of $\psi_{2,\max}/Ma$ as a function of $1/\kappa^*$ (Pr_1/Pr_2) for different values of Ma, in the case of Fig. 5.

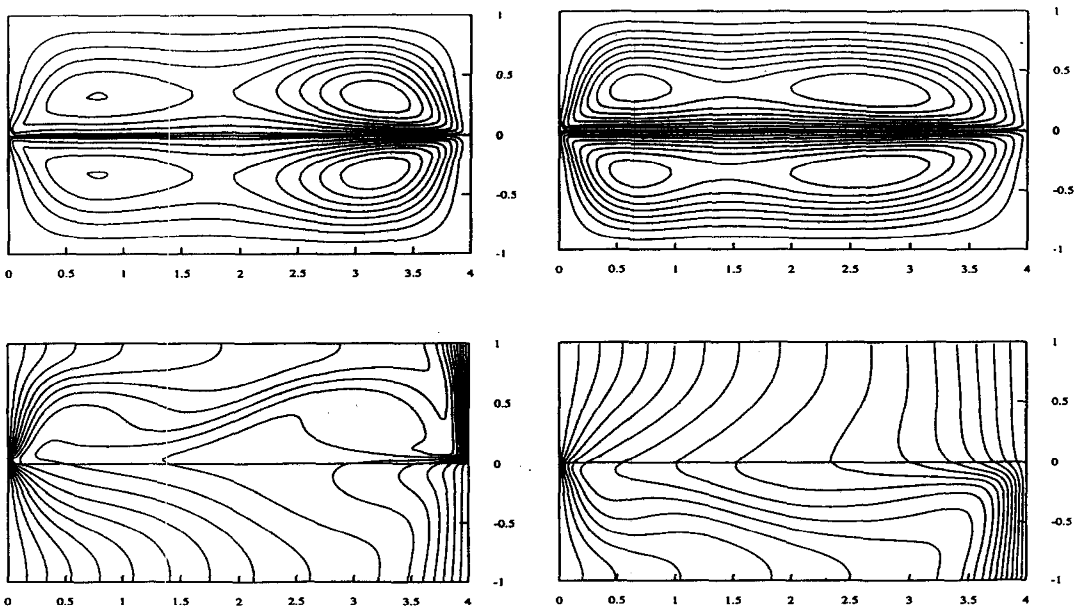

(a) (b)

Fig. 5. Streamlines (above) and isotherms (below) for asymmetric systems ($\kappa_1 \neq \kappa_2$) at $Pr_2 = h^* = \mu^* = \rho^* = \lambda^* = 1$ and $A = 4$; (a) for $\kappa^* = 0.1$, $Ma = 500$; (b) for $\kappa^* = 10$, $Ma = 1000$.

the same in each layer (same viscosity, same geometry). However, the thermal fields are different in the two layers (see Fig. 5(a)–(b)); isotherm patterns change much more strongly in the liquid layer whose thermal diffusivity is weaker. The flow intensity differs from that in case $\kappa^* = 1$. It depends on κ^* as the thermocapillary forces are proportional to the temperature gradient along the interface, that couples the Navier–Stokes equations and the energy equation.

Figure 6 shows the evolution of the maximum streamfunction in the melt as a function of the thermal diffusivity ratio (κ^*) for different Marangoni numbers. Note that the asymptotic solution given by expression (18), which is also plotted in Fig. 6 (solid line), does not depend on the thermal diffusivity ratio κ^*. For the 1-D solution (infinite aspect ratio) the longitudinal temperature gradient is constant (not coupled with the dynamics). But, as it can be seen in Fig. 5(a) for $\kappa^* = 0.1$, the 2-D numerical solutions show that the temperature distribution along the interface is strongly affected when the encapsulant has a lower diffusivity. The longitudinal temperature gradient decreases at the centre and increases near the endwalls hence reducing convective flow in the system. For $\kappa^* = 10$ (Fig. 5(b)), the situation is the opposite; for the same Ma the convective flow is stronger than for $\kappa^* = 0.1$, as the temperature gradient along the interface is more uniform. In fact, for small Ma the flow velocity tends to the 1-D solution.

3.4. *Concluding remarks*

Summing up, for the confined geometry (the cavity with a rigid top-wall) and for two liquid layers of equal depth ($h^* = 1$), we can safely say (see Figs. 4–6) that to reduce the mass flow rate in the melt layer there is interest in using an encapsulant liquid of higher viscosity than the melt (which yields viscous damping), and/or with lower thermal diffusivity than the melt (which reduces thermocapillary convection by lowering the temperature gradient along the interface, in the centre of the cavity).

4. THE B_2O_3–GaAs SYSTEM

In this section, we consider the case of molten GaAs encapsulated by B_2O_3. The physical properties of the fluids are listed in Table 2. We study two cases: (i) rigid top surface (case A) and (ii) an open, free top surface subject to the Marangoni thermocapillary force (case B). For case B, we also consider that surface-tension temperature coefficient at the top surface $(-\partial\sigma_{1-\mathrm{air}}/\partial T)$ can be varied while the corresponding coefficient at the interface $(-\partial\sigma_{2-1}/\partial T)$ is fixed.

4.1. *The B_2O_3–GaAs in a cavity with no open surface (case* A)

The thermocapillary convection for a B_2O_3–GaAs system has been investigated for two aspect ratios ($A = 2$ and $A = 4$) and Marangoni numbers ranging from $Ma = 750$ to $Ma = 6\times10^4$. The results concerning the mass flow rate $\psi_{2,\max}$ in the melt and the maximum interfacial velocity are plotted in Fig. 7(a)–(b), respectively, in terms of Ma in the range $750 < Ma < 15\,000$. In this range, the mass flow rates in the encapsulant layer $|\psi_{1,\min}|$ and in the melt $\psi_{2,\max}$ are nearly the same. This result is connected to the fact that the isotherms are only slightly deviated from the ones of the motionless, conducting regime. According to equation (18), it would be more relevant to express the mass flow rate in terms of the Marangoni number divided by $\mu^* = 1398$. Then the results of Fig. 7 would be in the range $0 < Ma/\mu^* < 11$, and we see that this linear variation of $\psi_{2,\max}$ agrees well with the results plotted in Fig. 2 for $\mu^* = 1$.

Figure 8(a)–(b) give streamlines and isotherms in a ($A = 4$) cavity for $Ma = 1500$ and $Ma = 6\times10^4$, respectively. In all cases, two counter-rotating convective cells fill the whole cavity, one in each layer. The two cells have almost the same intensity (maximum stream-function) for low Marangoni numbers. The horizontal velocity profiles at $x = 0.5A$, in the two layers are symmetric with respect to the interface. This is in agreement with the theoretical velocity profiles obtained for infinite aspect ratio layers ($A \to \infty$) when $h^* = 1$ ([11]). The form of the convective cell in the encapsulant almost does not change and that in the

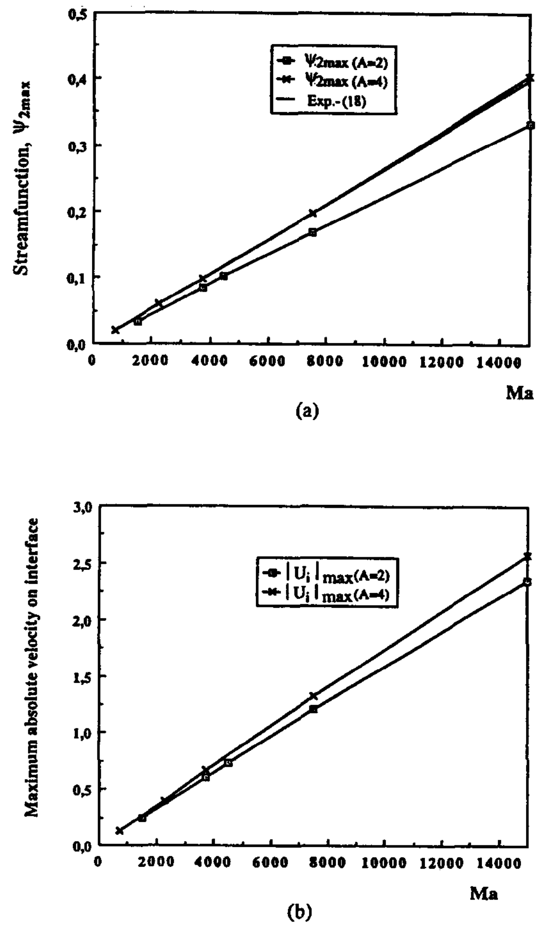

Fig. 7. Variation of $\psi_{2,\max}$, (a); and maximum absolute values of the velocity at the interface, (b); as a function of Ma, in case A; for $A = 2$, and $A = 4$, $h^* = 1$.

Table 2. Physical properties of the B_2O_3 liquid and the GaAs liquid

Fluid	κ [m²/s]	λ [W/m/K]	μ [kg/m s]	ν [m²/s]	ρ [kg/m³]	β [K⁻¹]	Pr
B_2O_3	2.52×10^{-6}	2.0	3.9	2.37×10^{-3}	1648	9.0×10^{-5}	939.1
GaAs	7.17×10^{-6}	17.8	2.79×10^{-3}	4.90×10^{-7}	5720	1.87×10^{-4}	0.068
B_2O_3/GaAs	0.352	0.112	1398	4829	0.288	0.481	13 741

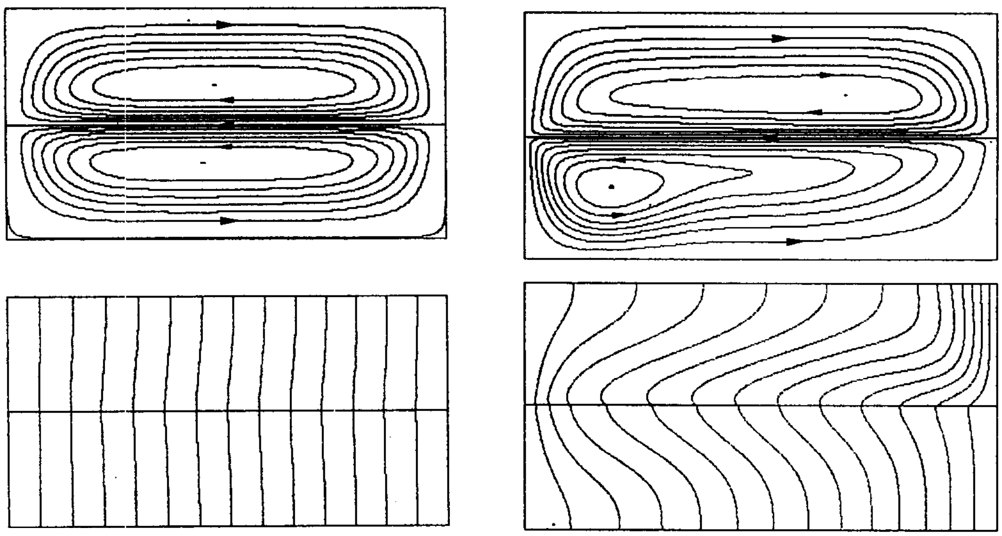

(a) (b)

Fig. 8. Streamlines (above) and isotherms (below) for case A, for $A = 4$, $h^* = 1$ at: (a) $Ma = 1500$ ($\psi_{max} = 3.9707 \times 10^{-2}$, $\psi_{min} = -3.9639 \times 10^{-2}$); and (b) $Ma = 6 \times 10^4$ ($\psi_{max} = 1.5265$, $\psi_{min} = -1.3282$).

melt is significantly modified (with the cell centre moving towards the cold sidewall). At the same time, the change of the temperature field in the encapsulant is stronger than in the melt, due to the very high Prandtl number of the B_2O_3 liquid. The form of the concentrated convective cell ('flywheel' structure) occurring in the GaAs layer at $Ma = 6 \times 10^4$ is similar to the one numerically found by Ben Hadid and Roux [19] for a single liquid layer with a low-Prandtl-number ($Pr = 0.0015$). Moreover, in our two-layer system, one may observe that the tendency of the flow towards the 'flywheel' structure in the melt is reduced relative to the case of a single liquid layer, due to the damping effect induced by the highly viscous B_2O_3 fluid. Thus both the high Prandtl number, and the high viscosity of the encapsulant liquid drastically affect the thermocapillary flow.

We have also investigated the influence of encapsulant layer thickness upon the melt flow for $A = 4$ and $Ma = 3750$, for fixed melt layer depth ($h_2 = 1$) while the thickness of the encapsulant is varied from 0.33 to 2. The evolution of $|\psi_{1,min}|$ ($|\psi_1|_{max}$) and $\psi_{2,max}$ are plotted in Fig. 9(a) in terms of the thickness ratio of the two layers. One observes that the convective flow, not only in the encapsulant but also in the melt, becomes less and less strong when h_1 decreases. This is consistent with expression (18) that shows that $\psi_{2,max}$ is proportional to h_* for large μ^*. Note that two counter-rotating cells still fill the whole cavity, but their intensity is no longer the same as soon as $h^* \neq 1$, in accordance with expression (17) that shows that $|\psi_{1,min}|$ is proportional to $h^2{}_*$ for large μ^*. This is shown in Fig. 9(b) where the dimensionless horizontal velocity profiles on the vertical mid-plane are plotted.

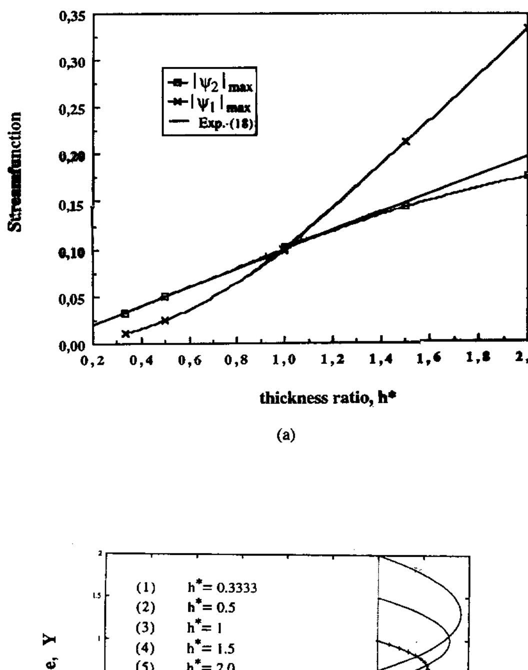

(a)

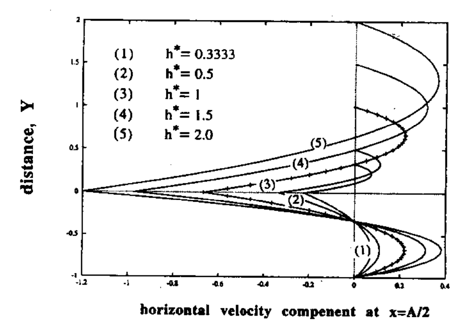

(b)

Fig. 9. Case A; (a) evolution of $|\psi_2|_{max}$ and $|\psi_1|_{max}$, for different values of h^*; (b) horizontal velocity profiles on the vertical mid-plane; for (1) $h^* = 0.33$; (2) $h^* = 0.5$; (3) $h^* = 1$; (4) $h^* = 1.5$; (5) $h^* = 2$, at $A = 4$, $Ma = 3750$ and $h_2 = 1$.

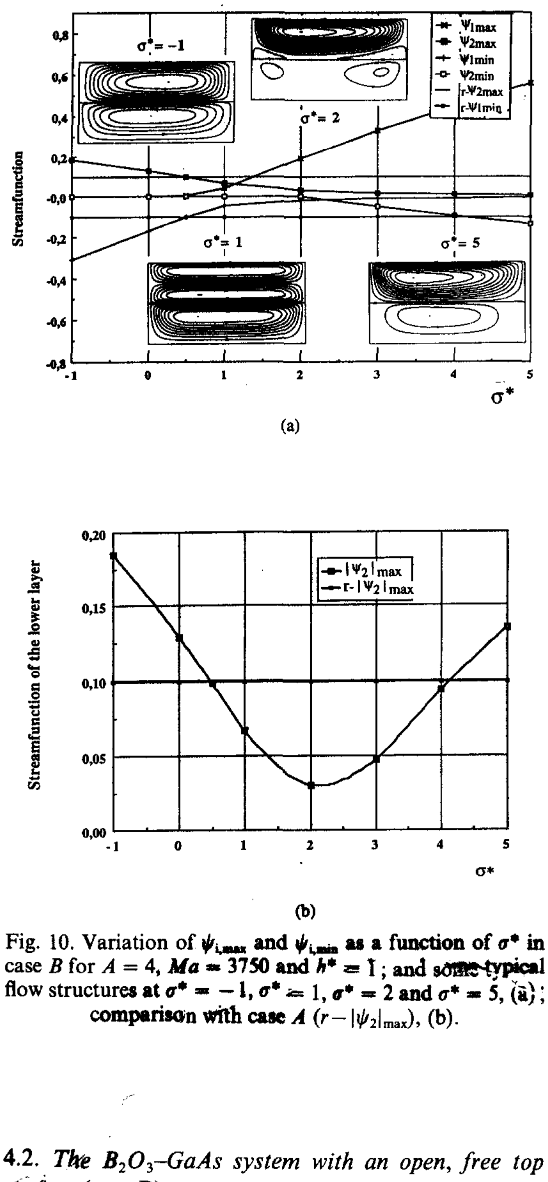

Fig. 10. Variation of $\psi_{i,\max}$ and $\psi_{i,\min}$ as a function of σ^* in case *B* for $A = 4$, $Ma = 3750$ and $h^* = 1$; and some typical flow structures at $\sigma^* = -1$, $\sigma^* = 1$, $\sigma^* = 2$ and $\sigma^* = 5$, (a); comparison with case *A* $(r-|\psi_2|_{\max})$, (b).

4.2. *The B_2O_3–GaAs system with an open, free top surface* (*case* B)

Now we consider the case of a B_2O_3–GaAs system open to air, when the Marangoni thermocapillary force acting on the open surface of the encapsulant is expected to influence the convective flow in both layers (case *B*). The direction and magnitude of this second thermocapillary force can be different from that at the encapsulant-melt interface. The quantity σ^* [see equation (14)] accounts for the ratio of the two surface tension parameters.

Numerical simulations of this two-layer system have been done for different σ^* but for a fixed value of $(-\partial\sigma_{2-1}/\partial T)$. Some typical flow structures are given in Fig. 10(a) for $-1 \leqslant \sigma^* \leqslant 5$ with $A = 4$, $h^* = 1$ and $Ma = 3750$. The streamfunction fields and horizontal velocity profiles in the vertical mid-plane are plotted. The flow direction in each layer is changed as a consequence of the coupling between the two thermocapillary forces. For $\sigma^* > 3$, there is one clockwise cell in the melt layer and one anti-clockwise in the encapsulant. For $\sigma^* < 0$ we have the opposite structure. The flow direction is imposed by the thermocapillary force along the top surface. For intermediate values of σ^*, the flow pattern is more complex; the encapsulant layer is filled with two counter-rotating cells for $\sigma^* = 1$. For $\sigma^* \approx 2$ the flow along the encapsulant-melt interface is reduced. In the latter case the thermocapillary effect along this interface is counter-balanced by the dynamical effect (viscous) induced by the anti-clockwise flow due to the thermocapillary effect along the top surface. Concurrently, the flow in the melt is very weak in comparison with that found in case *A* (see Fig. 10(a) for $\sigma^* = 2$).

A comparison of flow characteristics in the melt, for case *A* and for several values of σ^* in case *B*, is given in Fig. 10(b), for $A = 4$ and $Ma = 3750$. We see that in the range $0.5 < \sigma^* < 4$ the mass flow rate in the melt ($\psi_{2,\max}$) for case *B* is lower than the one for case *A*; the optimum is obtained for $\sigma^* \approx 2$, where there is a reduction by a factor of 3. Two other numerical computations of the same case have been performed for $Ma = 1250$ and $Ma = 7500$, respectively. We also found that it exists a range of values of σ^* where the mass flow reduction in the melt layer is more effective than in the case of a rigid top surface. The upper limit of σ^*, denoted $\sigma^*_{\lim}$, slightly increases with *Ma*, but it is not less than 3.5 (which corresponds to the analytical result for an infinite aspect-ratio system, $A \to \infty$).

Like case *A*, increasing (or decreasing) the encapsulant thickness in case *B* greatly affects the flow intensity in the melt layer for every value of σ^*. Numerical experiments were performed for $\sigma^* = 2$ by varying h^* from 0.33 to 2 in the case of B_2O_3–GaAs system with $A = 4$, $h_2 = 1$ and $Ma = 3750$. The computed results reported in Fig. 11(a–b) show that the convective flow in the melt layer is much weaker for $h^* = 0.33$ than for $h^* = 1$. Conversely, when $h^* > 1$, the greater the upper layer thickens, the more the flow velocity increases in the melt layer. The same behaviour was observed in Fig. 9(b) for case *A*. The intensity of the intermediate cell (staying always near the interface in the encapsulant), becomes noticeably stronger when the thickness of the encapsulant increases. Then, the melt layer is not completely at rest, even for $\sigma^* = 2$. This means that the damping effectiveness of the thermocapillary top surface on the melt motion depends not only upon a suitable choice of σ^* (physical condition), but also upon an appropriate choice of the thickness of the encapsulant (geometrical condition).

Finally, we have paid special attention to the melt flow structure for different aspect ratios (for $1 \leqslant A \leqslant 12$), also in case *B* for $\sigma^* = 2$. For illustration, we have taken: $h^* = 1$ and $Ma = 3750$. To maintain the Marangoni number constant, the external temperature gradient is taken constant (i.e., ΔT is varied proportionally to *A*). The velocity profiles at the interface are plotted in Fig. 12 for several values of *A* (1, 2, 4, 6, 8, 10 and 12). Four flow patterns, corresponding, respectively, to $A = 1, 2, 6$ and 12, are

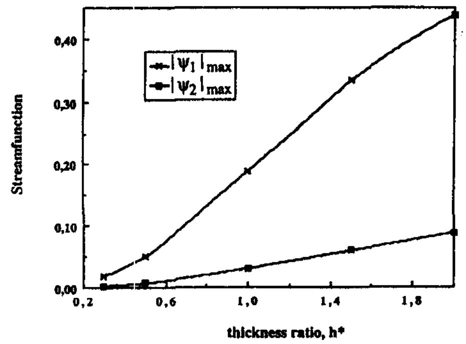

(a)

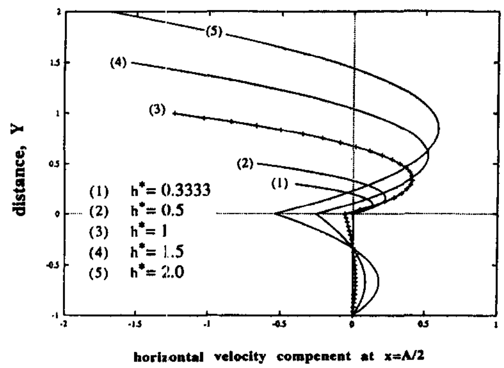

(b)

Fig. 11. Case B; (a) evolution of $\psi_{1,\max}$ and $\psi_{2,\max}$ as a function of h^*; (b) horizontal velocity profiles on the vertical mid-plane; for (1) $h^* = 0.33$; (2) $h^* = 0.5$; (3) $h^* = 1$; (4) $h^* = 1.5$; (5) $h^* = 2$, at $A = 4$, $\sigma^* = 2$, $Ma = 3750$ and $h_2 = 1$.

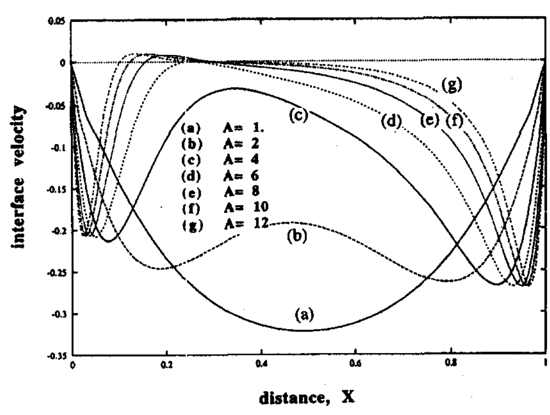

Fig. 12. Evolution of velocity profiles at the interface as a function of A, for case B at $\sigma^* = 2$, $Ma = 3750$ and $h^* = 1$, (a) $A = 1$; (b) $A = 2$; (c) $A = 4$; (d) $A = 6$; (e) $A = 8$; (f) $A = 10$; (g) $A = 12$.

given in Fig. 13 for $\sigma^* = 2$ (for $A = 4$ see Fig. 10(a)). For smaller aspect ratios ($A < 4$) an intermediate cell appears in the encapsulant and flow exists in the whole melt layer. For larger and larger A, the intermediate cell (near the two endwalls) is less and less observable and the melt flow is more and more effectively reduced in the central region of the cavity. For $A > 8$, the largest cell in the melt splits into two smaller counter-rotating vortices near the two lateral walls of the cavity where there still exists a high velocity gradient (along the interface) due to the relatively high interfacial tension gradient. It is noticeable that the melt mass flow rate is almost independent of the cavity aspect ratio ($\psi_{2,\max} \approx 3.03 \times 10^{-2} \pm 0.03 \times 10^{-2}$; for $1 \leqslant A \leqslant 12$).

4.3. *Influence of the viscosity of the encapsulant*

In the previous section we considered the system B_2O_3–GaAs with a highly viscous encapsulant ($\mu^* = 1398$). Here, we complement this study by numerically studying in further depth the influence of encapsulant viscosity in a wide range of values of μ^* while keeping μ_2 constant. For $A = 4$, $\sigma^* = 2$, $h^* = 1$ and $Ma = 250$, the computed values of $\psi_{\max}$ are plotted in Fig. 14. When decreasing μ^* by a factor 1000, thermocapillary convection becomes stronger in both encapsulant and melt layers, and the damping of the melt motion becomes weaker. For $\mu^* = 1398$, the mass flow rate in the melt ($\psi_{2,\max}$) is about an order of magnitude smaller than in the encapsulant ($\psi_{1,\max}$). This difference is reduced to a factor two only for $\mu^* = 1.398$. In fact, $\psi_{2,\max}$ for $\mu^* = 1.398$ increases about three orders of magnitude relative to the case $\mu^* = 1398$. The curve plotted in Fig. 14 shows that the mass flow rate in the melt ($\psi_{2,\max}$) is inversely proportional to μ^*. Note that this behaviour is the same as in the rigid top-boundary (case A), as discussed in Section 3.2 (where expression (8) applies). In addition, these results show that even for the special situation when $\sigma^* = 2$ (i.e., when thermocapillary forces at the encapsulant-melt surface and at the open, free top surface are in balance). Thus a highly viscous encapsulant helps to strongly reduce motion in the melt.

The effect of a highly viscous encapsulant can also be seen by comparing the flow structures at $\mu^* = 1.398$ and at $\mu^* = 1398$ (see Fig. 14). For $\mu^* = 1.398$, the intermediate convection cell in the upper layer near the liquid–liquid interface appears quite nearly and its intensity becomes much greater than at $\mu^* = 1398$, even for the special case of $\sigma^* = 2$.

5. SUMMARY AND CONCLUSION

A numerical investigation of pure thermocapillary convection ($g = 0$) has been carried out for two immiscible liquid layers in a rectangular cavity subject to a temperature gradient parallel to the liquid–liquid interface. In the simpler case of rigid top boundary, a true cavity, the influence of viscosity ratio and of diffusivity ratio of the two layers has been investigated for various fluids. We even considered the unrealistic

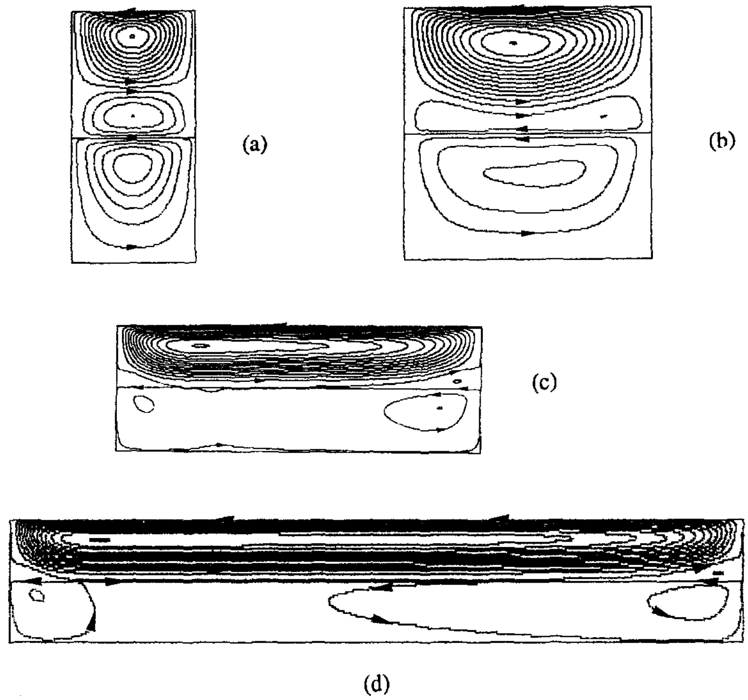

Fig. 13. Steady flow structures in case *B* for different aspect ratios of the lower layer, at $\sigma^* = 2$, $Ma = 3750$ and $h^* = 1$, (a) $A = 1$; (b) $A = 2$; (c) $A = 6$; (d) $A = 12$; for $A = 4$ see in Fig. 10(a). ($\sigma^* = 2$.)

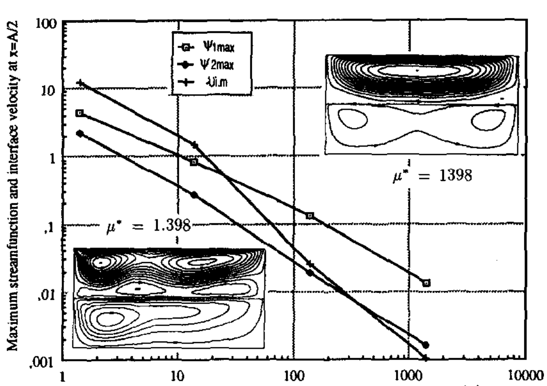

Fig. 14. Variation of $\psi_{i,\max}$ and (absolute) horizontal velocity at $x = A/2$ on the interface as a function of μ^*, and two typical flow structures at $\mu^* = 1398$ and $\mu^* = 1.398$, for case *B* at $A = 4$, $\sigma^* = 2$, $Ma = 3750$, $h^* = 1$ and $\mu_2 = 2.79 \times 10^{-3}$.

case of a 'symmetric' system (with equal diffusivity and viscosity in each layer; but with a temperature dependence of surface tension). In such a case, the flow structure and temperature fields are found to be perfectly symmetric with respect to the interface. For asymmetric systems with different thermal diffusivities ($\kappa_1 \neq \kappa_2$) but equal viscosity, the flow is symmetric while the temperature field is not, as expected. For asymmetric systems with different viscosities ($\mu_1 \neq \mu_2$), both velocity field and temperature field are asymmetric. Increasing viscosity or reducing diffusivity in the encapsulant layer helps reduce the convection intensity in the melt with higher efficiency in the former than in the latter case.

The experimentally relevant case of a B_2O_3–GaAs system was studied for two top surface conditions: either rigid or free but subject to thermocapillary forces. A comparison has been performed between these two cases. For case *B* there exists a range of σ^* in which the flow in the melt is less than that for a rigid top surface (case *A*). The melt flow damping is almost maximum for $\sigma^* = 2$ where it reaches a factor of 3, for an aspect ratio $A = 4$. The damping for $\sigma^* = 2$ is still efficient for a large range of aspect ratios ($1 \leqslant A \leqslant 12$). Despite this clear advantage of case *B*, case *A* is probably simpler to implement for technological applications.

Thermocapillary convection in the melt layer is highly influenced by the thickness of the encapsulant layer in both cases (*A* and *B*). A thinner encapsulant layer is more efficient to reduce the melt motion. However, technological limitation to this reduction is the possible rupture of the encapsulant film, particularly catastrophic in case *B*.

As a general conclusion we can safely say that the mass flow rate in the melt is inversely proportional to the encapsulant viscosity whatever the geometry used, a cavity or a two-layer system open to air (cases *A* and B). The use of a highly viscous encapsulant appears best to significantly reduce the intensity of thermocapillary convection in the melt. Finally, the relationship (18) can be very useful as a guide for practical purposes.

Acknowledgements—This research was supported by the Centre National d'Etudes Spatiales (Division Fluides et Materiaux en Microgravite), by HCM European Network Heat and Mass Transfer in non-homogeneous systems (Contract No. 930106), by AFCRST (France) under grant PRA M94-02, and by DGICYT (Spain) under grant PB93-81. The computations were carried out on Intel-iPSC/860 of IRPHE.

REFERENCES

1. Metz, E. P. A., Miller, R. C. and Mazelsky, R., A technique for pulling single crystals of volatile materials. *Journal of Applied Physics*, 1962, **33**, 2016–2017.
2. Johnson, E. S., Liquid encapsulated floating zone melting of GaAs, *Journal of Crystal Growth*, 1975, **30**, 249–256.
3. Barocela, E. and Jalilevand, A., Liquid encapsulated float zone method for microgravity production of gallium arsenide. AIAA-87-0390, 1987.
4. Villers, D. and Platten, J. K., Thermal convection in superposed immiscible liquid layers. *Applied Scientific Research*, 1988, **45**, 145–151.
5. Villers, D. and Platten, J. K., Influence of interfacial tension gradients on thermal convection in two superposed immiscible liquid layers. *Applied Scientific Research*, 1990, **47**, 177–191.
6. Koster, J. N., Praskash, A., Fujita, D. and Doi, T., Benard and Marangoni convection in multiple liquid layers. *Proceedings of the VIIIth European Symposium on Materials and Fluid Sciences in Microgravity*. Brussels, Belgium, 1992, ESA SP-333, pp. 221–226.
7. Azuma, H., Yoshihara, S., Ohnishi, M. and Doi, T., Upper layer flow phenomena in two immiscible liquid layers subject to a horizontal temperature gradient. *Microgravity Science Technology*. Hanser Publisher, Munich, 1991, IV/2, pp. 154–155.
8. Napolitano, L. G., Viviani, A. and Savino, R., Natural and Marangoni convection in two superposed immiscible fluid layers with horizontal heating. *Proceedings of the First European Symposium on Fluids in Space*. Ajaccio, France, 1992, ESA SP-353, pp. 79–118.
9. Wang, C. H., Sen, M. and Vasseur, P., Analytical investigation of Bénard–Marangoni convection heat transfer in a shallow cavity filled with two immiscible fluids. *Applied Scientific Research*, 1991, **48**, 5–53.
10. Shevtsova, V. M., Indeikina, A. E. and Ryazantsev, Y. S., Thermocapillary motion of a two layered liquid with nonlinear dependence of the surface tension on the temperature. *Proceedings of the International Symposium on Hydromechanics and Heat/Mass Transfer in Microgravity*, Perm, Russia. Gordon and Breach Science Publ., 1992, pp. 157–162.
11. Liu, Q. S., Chen, G. and Roux, B., Thermogravitational and thermocapillary convection in a cavity containing two superposed immiscible liquid layers. *International Journal of Heat and Mass Transfer*, 1993, **36**, 101–117.
12. Doi, T. and Koster, J. N., Thermocapillary convection in two immiscible liquid layers with free surface. *Physics and Fluids A*, 1993, **5**, 1914–1927.
13. Liu, Q. S., The coupling between the interfacial forces in a system of multiple immiscible fluid layers, with or without the effect of the thermogravitational forces. Ph.D. Dissertation, Institut de Mecanique des Fluides de Marseille, Universite d'Aix-Marseille II (in French, available upon request; IRPHE–IMT, Technopole de Chateau-Gombert, F-13451 Marseille Cedex 20), 1994.
14. Crespo, E., Extremet, G. P. and Sani, R. L., Thermocapillary convection in a two-layer fluid system with flat interface. *Advances in Space Research*, 1991, **11**, 129–132.
15. Fontaine, J. P. and Sani, R. L., Thermocapillary effects in a multilayered fluid system. AIAA-92-0689, 1992.
16. Li, J., Sun, J., Saghir, Z. and Roux, B., Maximum stable zone length in floating zone melting of GaAs and effect of liquid encapsulation. *43rd Congress of the International Astronautical Federation*, Report IAF-92-0910, 1992, pp. 1–11.
17. Sen, A. K. and Davis, S. H., Steady thermocapillary flows in two-dimensional slots, *Journal of Fluid Mechanics*, 1982, **121**, 162–186.
18. Shevtsova, V. M., Fujiwara, T. and Ryazantsev, Y. S., Thermoconvection motion in a two-layer system. *Research Report*; *Memoirs of the Faculty of Eng., Nagoya University, Japan*, 1991, **43**, 113–120.
19. Ben Hadid, H. and Roux, B., Thermocapillary convection in long horizontal layers of low-Prandtl-number melts subject to a horizontal temperature gradient. *Journal of Fluid Mechanics*, 1990, **211**, 77–103.